B. Damiens
Laboratoire de Mécanique des Contacts,
UMR CNRS 5514,
INSA de Lyon, France

C. H. Venner
University of Twente,
Tribology Group,
The Netherlands

P. M. E. Cann
Department of Mechanical Engineering,
Tribology Section,
Imperial College,
London SW7 2BX, UK

A. A. Lubrecht
Laboratoire de Mécanique des Contacts,
UMR CNRS 5514,
INSA de Lyon, France

Starved Lubrication of Elliptical EHD Contacts

This paper focuses on the lubrication behavior of starved elliptical Elasto-HydroDynamic (EHD) contacts. Starvation is governed by the amount of lubricant available in the inlet region and can result in much thinner films than occurring under fully flooded conditions. Therefore, it would be desirable to be able to predict the onset and severity of starvation and to be able to relate film reduction directly to the operating conditions and lubricant properties. The aim of this work is to explore the influence of these parameters on starvation. A combined modeling and experimental approach has been employed. The numerical model has been developed from an earlier circular contact study [1]. In this model, the amount and distribution of the lubricant in the inlet region determines the onset of starvation and predicts the film decay in the contact. Numerical simulations for a uniform layer on the surface show that a single parameter, characteristic of the inlet length of the contact in the fully flooded regime, determines the starved behavior. Film thickness measurements under starved conditions were performed to validate this theory. For a circular contact excellent agreement was found. In theory the same mechanism applies to elliptic contacts, however, the behavior is more complicated.
[DOI: 10.1115/1.1631020]

1 Introduction

The past century has seen a considerable improvement in the performance of machine elements. The average pressure, speed, temperature, accuracy and life have increased as the size, weight, and cost have decreased. This has been accomplished through improved design and manufacture, and advances in lubrication. A second factor however is the reduction of safety margins. One consequence of this reduction is that increasingly accurate predictions of all operational parameters are required, including lubricant performance, to prevent component failure.

The foundation of modern quantitative lubrication theory was laid by Dowson and Higginson in 1959 [2] and Hamrock and Dowson in 1976 [3]. They studied the lubricant film generated between the contacting bodies. The main characteristic of this film is its thickness which plays a crucial role in determining the life of the contact. Hamrock and Dowson studied the film thickness as a function of speed, load, geometry, material, and lubricant properties under fully flooded conditions. The ensuing relation has been validated experimentally on many occasions. However under more realistic conditions, for example with rough surfaces or under nonsteady state conditions, the film behavior is more complex.

One of the most important aspects still to be understood is the problem of starvation, where the amount of lubricant available is insufficient to fill the inlet conjunction. Under these conditions the film thickness is often much less than predicted by fully flooded theory. Starvation can be due to excessive speeds, high lubricant viscosity or a limited amount of lubricant present. In all cases this contributes to a reduction in the amount of lubricant replenishing the rolled track. Thus starvation is common in grease lubricated, high speed or large bearings.

Starvation is usually studied in a ball-on-plate optical device [4]. In these tests, film thickness is measured as a function of speed (Fig. 1). The film thickness h increases initially with speed u according to the classical (fully flooded) relationship ($h \propto u^{0.67}$ for a point contact). But from a certain critical speed onwards, the film thickness starts to decrease with increasing speed ($h \propto u^{-1}$); the starved regime. In this regime, insufficient lubricant is available in the inlet of the contact, resulting in reduced film buildup. Starved lubrication has been studied by Wedeven [4], Pemberton, Evans, and Cameron [5], and Kingsbury [6]. Experimental observations show that under these conditions, the air-oil meniscus moves closer to the Hertzian radius as the speed increases. Hence, the position of the inlet meniscus was used as the parameter governing starvation. There are two disadvantages concerning this criterion. Firstly, this length is difficult to measure in an industrial application, as it is hidden by the rolling element. Secondly, when the contact becomes heavily starved the inlet meniscus coincides with the hertzian radius, thereby rendering this inlet criterion of little use.

Theoretical studies include the work by Chiu [7], Kingsbury [6], and more recently Guangteng [8] and Chevalier [1]. Chevalier used the thickness of the oil layer on the track as a primary parameter. This parameter relates more directly to the thickness of the film in the center of the contact. They are of the same order under heavily starved conditions (neglecting oil compressibility).

Most of the early work has concentrated on studying circular contacts. However, elliptical contacts, for example in roller bearings, are likely to be of more practical importance as such contacts are more common and more susceptible to starvation. This paper extends the circular model developed by Chevalier [1] to an elliptical geometry and attempts to give a physical explanation for the observed behavior. The model has been verified by a parallel experimental study, where film thickness under starved conditions has been measured in a roller on disc optical test device.

The critical factor determining the onset of starvation is the balance of lubricant loss from, and replenishment to, the inlet. The first step in understanding this balance is to understand the ejection of the lubricant. An experimental technique to study this ejection is to run the contact under conditions of negligible reflow (high base oil viscosity and small amounts of fluid), and to study the film reduction. This experiment can be easily modeled numerically, and the results compared.

The problem has been modeled both numerically and through an analytical approach. The numerical model simulates the dimensionless film thickness reduction for each overrolling of the track. The film thickness reduction law depends on a single parameter (coined γ in [1]). The analytical model gives a prediction of this parameter, based on physical assumptions concerning the poiseuille flow in the inlet.

Contributed by the Tribology Division for publication in the ASME JOURNAL OF TRIBOLOGY. Manuscript received by the Tribology Division May 8, 2002 revised manuscript received October 8, 2002. Associate Editor: L. Chang.

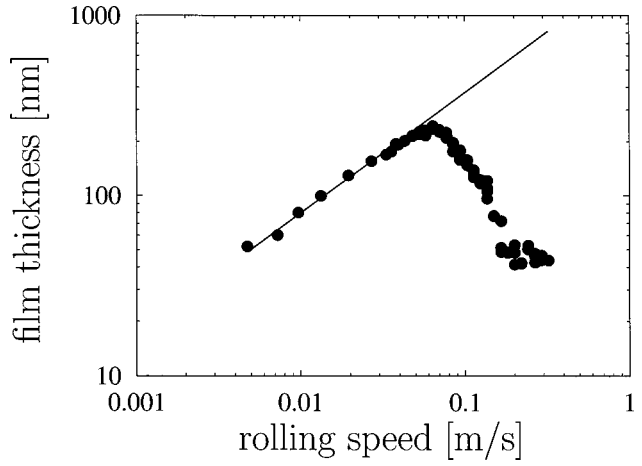

Fig. 1 Film thickness as a function of speed (circular contact)—starvation occurs at 0.06 [m/s], full line $h \propto u^{0.67}$

2 Theory

The model developed by Elrod [10,11] is used to describe the lubricant flow in the contact. This model divides the calculational domain into two sub-domains. In the first zone the gap is completely filled with lubricant, the pressure is positive and the traditional Reynolds equation applies. In the other region, two lubricant layers, separated by an air layer, stick to the ball and the disk. The lubricant layers are moving with the surfaces and the pressure is zero. A parameter θ (filling rate) representing the ratio of the oil thickness and the gap is introduced in the Reynolds equation which becomes valid in the entire domain using: $0 \leqslant \theta < 1$, $P=0$ or $\theta=1$, $P>0$.

Capillary forces causing the reflow of the lubricant are neglected.

2.1 Equations. Wijnant [12] studied the starved elliptical contact and derived the corresponding dimensionless Reynolds equation (1).

The dimensionless parameters for an elliptical contact are defined in the nomenclature. Over the dimensionless domain $\mathcal{D}$ (see Fig. 2), the resulting dimensionless Reynolds equation reads:

$$\frac{\partial}{\partial X}\left(\frac{\overline{\rho}\overline{H}^3}{\overline{\eta}\lambda}\frac{\partial P}{\partial X}\right)+\kappa^2\frac{\partial}{\partial Y}\left(\frac{\overline{\rho}\overline{H}^3}{\overline{\eta}\lambda}\frac{\partial P}{\partial Y}\right)-\frac{\partial(\overline{\rho}\theta H)}{\partial X}=0 \qquad \mathcal{D}: X_0 \leqslant X \leqslant X_e, -Y_0 \leqslant Y \leqslant Y_0 \tag{1}$$

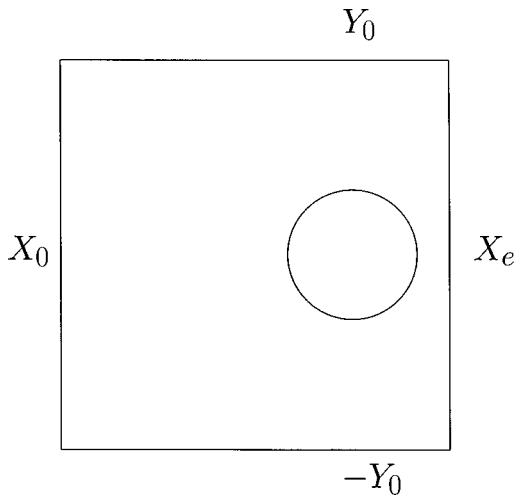

Fig. 2 Elliptical contact in the dimensionless domain $\mathcal{D}$

With the boundary conditions:

$$P(X_0,Y)=P(X_e,Y)=P(X,-Y_0)=P(X,Y_0)=0$$

and

$$\theta(X_0,Y)=H_{\text{oil}}(Y)/H(X_0,Y).$$

And the complementarity equation:

$$0 \leqslant \theta < 1 \quad \text{and} \quad P=0 \quad \text{(incomplete film)} \tag{2}$$

$$\theta=1 \quad \text{and} \quad P>0 \quad \text{(complete film)} \tag{3}$$

The dimensionless gap between the surfaces is given by

$$H(X,Y)=H_0+\mathcal{S}X^2+(1-\mathcal{S})Y^2+\frac{1}{\pi\mathcal{K}}\int\int_{\mathcal{D}}\frac{P(X',Y')dX'dY'}{\sqrt{\kappa^2(X-X')^2+(Y-Y')^2}} \tag{4}$$

The dimensionless rigid body displacement H_0 is coupled to the force balance equation which, for an elliptical contact reads

$$\int\int_{\mathcal{D}}P(X,Y)dXdY=\frac{2\pi}{3} \tag{5}$$

The viscosity pressure relation proposed by Roelands is used

$$\overline{\eta}(P)=\exp\left\{\frac{\alpha p_0}{z}\left(-1+\left(1+\frac{Pp_h}{p_0}\right)^z\right)\right\} \tag{6}$$

with

$$\frac{\alpha p_0}{z}=\ln\eta_0+9.67 \tag{7}$$

The compressibility is taken into account using the density pressure relation proposed by Dowson and Higginson

$$\overline{\rho}(P)=\frac{0.5910^9+1.34Pp_h}{0.5910^9+Pp_h} \tag{8}$$

2.2 Analytical Approach. The pressure buildup in the inlet of the contact starts far before the hertzian radius. In the Ertel Grubin [13,14] analysis it starts at an infinite distance. In his thesis (page 192 equation (6.17)) Wedeven [15] derived the relation (9) between the inlet distance s and the film thickness in the contact (which is assumed to be constant in the Hertzian region and equal to h_c).

$$\frac{h_c}{R_x}=\frac{4}{3}\left(\frac{\alpha\eta_0 u}{R_x}\right)^{1/2}\left(\frac{s}{R_x}\right)^{1/2} \tag{9}$$

This film thickness can be equated to the film thickness (10) predicted by Moes [9]. In the Elastic Piezoviscous regime, the behavior of the film thickness can be approximated according to Moes by its asymptote.

$$H_{ep}^M=C_{ep}M^{-1/12}L^{3/4} \tag{10}$$

For each set of parameters (M and L), the system of equations formed by (9) and (10) determines the only unknown s_{ff} which is the characteristic inlet length of the fully flooded regime.

$$\frac{s_{ff}}{a}\propto\left(\frac{L}{M}\right)^{1/2} \tag{11}$$

This characteristic length represents the size of the domain where a significant poiseuille component of the flow exists. The poiseuille flow removes the lubricant from the track. Hooke and Venner [16] derived a similar length in order to characterize the roughness amplitude reduction.

A lack of lubricant in the inlet will significantly affect the central film thickness as soon as the distance between inlet meniscus and the Hertzian radius becomes smaller than s_{ff}.

The dimensionless inlet distance $\overline{S}=s_{ff}/a$ depends on the operating conditions and material properties and allows quantification of the side-flow. This is confirmed by Figs. 5 and 6 which gather the data on a unique curve.

In elliptical contacts, equating (9) and (10) leads to:

$$\overline{S}=\frac{s_{ff}}{a}\propto\left(\frac{\mathcal{E}}{\kappa(1+R_x/R_y)}\right)^{1/2}\left(\frac{L}{M}\right)^{1/2} \tag{12}$$

In [16] an elliptical inlet length similar to (12) was introduced, allowing a single amplitude reduction curve for all ellipticities.

3 Numerical Solution

In the region filled with lubricant ($\theta=1$) the equations are the same as in the fully flooded regime with a free exit boundary. The Multigrid/Multi Level Multi Integration technique [17], has been used to solve the system of nonlinear equations efficiently. The numerical details of the stationary starved point contact can be found in Chevalier [18] and for the elliptical contact in Wijnant [12]. A first order discretization has been implemented with a distributive line relaxation to increase the stability of the solver.

4 Numerical Results

The behavior of a given elasto-hydrodynamic contact across the starvation regime is characterized by the amount of oil that is removed from the overrolled track every time the rolling elements pass through the contact. This behavior can be reduced to one parameter called γ by Chevalier [1].

The aim of the present paper is to obtain the parameter γ as a function of the operating conditions. This can be done with the solver in two different ways. For a steady-state contact, from results obtained varying H_{oil} as input parameter to create a ''starvation curve,'' and from this curve γ is derived using the formula of Chevalier (13) and a least square fit. A second approach simulates repeated overrollings; for given conditions starting with some H_{oil}, solve the problem and feed the computed layer of oil in the outlet as input for the next simulation.

Both methods allow one to evaluate, for different oil quantities, the amount of oil removed from the track when it is overrolled. Hence, the γ parameter can be derived. Basically the principle is the same in both methods (evaluate the film reduction for different oil layers). For steady state contacts a number of representative oil quantities are chosen and the corresponding computations are performed with a flat inlet oil profile. Whereas in the overrolling method, the inlet oil profile is more physical. Nevertheless, to reach the very starved regime (i.e., tiny oil layers) many cycles must be computed until little lubricant remains on the track. This implies a large number of computations and makes the method very time consuming. Furthermore, a propagation of errors in the oil profile occurs. Using calculation with different mesh sizes, the discretisation error can be estimated. In this paper, it is of the order of 1% in γ.

4.1 Film Decay: Starvation Curve. Using the mathematical model allows one to impose the shape of the inlet oil profile h_{oil} and to deduce the position of the mobile inlet meniscus (free boundary problem). For each set of lubrication conditions (load, speed, viscosity, geometry, material, H_{oil}), the ratio $\mathcal{R}$ of the central film thickness H_c and fully flooded central film thickness H_{cff} can be computed. This parameter $\mathcal{R}=H_c/H_{cff}$ can be plotted as a function of the dimensionless oil thickness on the track $r=H_{\text{oil}}/(\overline{\rho}H_{cff})$, see Fig. 3. From Chevalier [1] a good approximation to this function is given by (13).

$$\mathcal{R}=\frac{r}{\sqrt[\gamma]{1+r^{\gamma}}} \tag{13}$$

Knowing γ and the thickness r of the oil layer, (13) allows one to predict the film thickness in the center of the contact. The remaining characteristic parameter of this approximation is thus $\gamma(\text{w,u,R}_x,\text{R}_y,\text{E}',\eta,\rho)$. The two straight lines in Fig. 3 represent the asymptotic behavior of $\mathcal{R}$. On the starved asymptote ($\mathcal{R}=r$ for $r\ll 1$) all the lubricant available on the track passes through the contact. On the fully flooded asymptote ($\mathcal{R}=1$ for $r\gg 1$) the excess oil layer ($h_{\text{oil}}-\rho(p_h)h_{cff}$) will flow around the contacting bodies. Only in two specific cases does a general contact follow these two asymptotes: a line contact or a point contact with $\gamma=\infty$. Thus the dimensionless parameter γ can be considered as a resistance to side-flow. $\gamma=\infty$ means no side-flow.

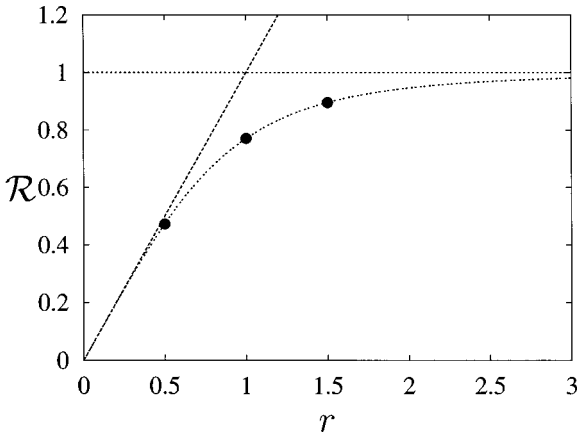

Fig. 3 $\mathcal{R}=f(r)$ for a circular contact with $M=10$ and $L=20$, $\gamma=2.66$

The dimensionless fully flooded film thickness H_{cff} and the compression $\overline{\rho}=\rho/\rho_0$ are known through the numerical solution of the fully flooded problem (Reynolds equation, elasticity equation, force balance equation). The three points of Fig. 3 are calculated by the starved code for $r=H_{\text{oil}}/(\overline{\rho}H_{cff})$ close to 1. The value of γ is deduced by a least squares approximation of the calculated points with the function (13).

In this way gamma has been computed for many different cases (characterized by M and L). In Fig. 4 the results obtained for a circular contact are shown. It can be seen that γ varies between 2 and 5. According to the theoretical model presented in Section 2.2, the parameter gamma should be a function of the $1/\overline{S}$, and thus $\gamma=f(\sqrt{M/L})$. This implies that when presented as a function of M/L the results should fall on a single line. This is illustrated by Fig. 5. The small deviations from the straight line that can be seen in this figure can be ascribed to numerical inaccuracy of the computed values. Furthermore, it should be kept in mind that the

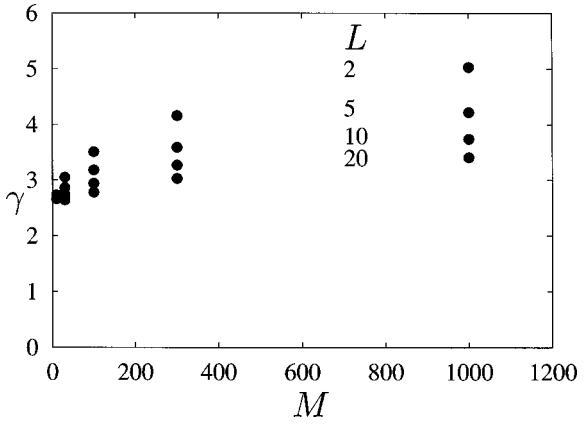

Fig. 4 γ as a function of M for a circular contact for $L=2, 5, 10, 20$, $r\simeq 1$

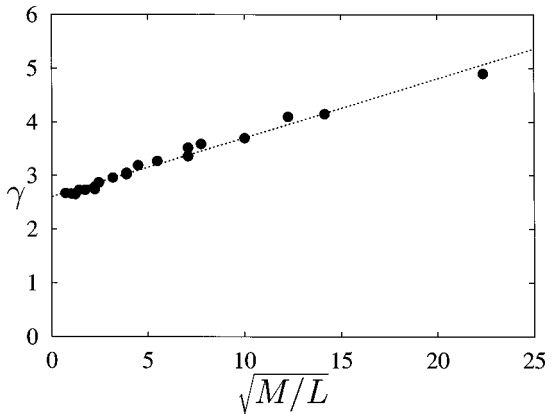

Fig. 5 γ **as a function of** $\sqrt{M/L}$ **for a circular contact for** $r \simeq 1$, $L=2, 5, 10, 20,$ **and** $M=10, 30, 100, 300, 1000$, $r \simeq 1$

relation between γ and M/L is only valid in the piezoviscous-elastic region, away from the isoviscous-elastic, isoviscous-rigid asymptotes.

The results plotted in Figs. 4 and 5 were obtained for a circular contact for various conditions of M and L. In the same way, the value of γ has been determined for elliptical contacts for different values of M, L, and κ. These results are presented in Fig. 6.

According to the theoretical model, the computed values of gamma, when presented as a function of $(M/L)^{1/2}$, should form a family of lines with the slope depending on the ellipticity parameter κ, which is indeed the trend shown by the results. Regarding the dependence of γ on the ellipticity it can be seen that for a given value of the parameter M/L, the value of γ increases with decreasing κ (increasingly wide ellipses). This means that the side flow is reduced when the ellipticity increases. This can be explained as follows: increasing ellipticity (reducing κ) reduces the pressure gradient in the y direction and increases the distance travelled by the lubricant to be ejected from the track.

The γ values presented in Figs. 4, 5, and 6, were obtained around $r \simeq 1$. However, the same analysis performed with smaller amounts of oil ($r \ll 1$) provides different γ values. Some results for the elliptical and the circular contact obtained with large and small amounts of oil are given in Table 1. This table shows that for a circular contact ($\kappa=1$), γ does not depend significantly on the amount of oil available on the track. However, a significant influence is obtained for the elliptical contact ($\kappa=0.14$). The difference between the γ obtained with an oil layer of $r \simeq 1$ and $r \simeq 0.2$ for the elliptical contact approaches a factor 2.

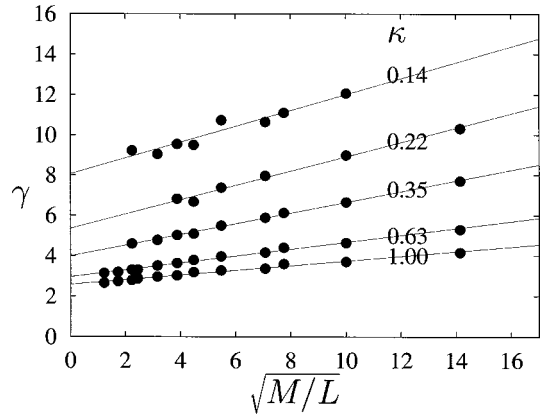

Fig. 6 γ **as a function of** $\sqrt{M/L}$ **for different ellipticities:** $\kappa = 0.14, 0.22, 0.35, 0.63, 1.00$, $r \simeq 1$

Table 1 γ **values obtained with different amounts of oil** r

κ	M	L	γ $0.5 \leqslant r \leqslant 1.5$	γ $0.1 \leqslant r \leqslant 0.3$
1	30	20	2.64	2.64
1	1000	20	3.36	3.03
0.14	100	20	9.19	4.75
0.14	1000	20	10.6	5.34

4.2 Film Decay: Repeated Overrolling. In Sec. 4.1 "single pass" calculations were performed to characterize starvation. In this section "multiple pass" calculations are performed that closely resemble the experimental procedure. Equation (13) relates the central film thickness to the thickness of the oil layer available on the track. Applying this equation recursively n times gives the reduction of the film thickness as a function of the number of passes n. Hence, in the model, the parameter γ controls the film reduction behavior.

It has been obtained numerically by computing fifty times the film thickness in the center of the contact using in the inlet the oil profile found in the outlet of the previous pass. Reference [1] determines the relation between the oil r in the inlet and the outlet $\mathcal{R}$. Between the passes: $r_{n+1}=\mathcal{R}_n$ with n the number of disk revolutions. An asymptotic behavior to (13) is found when n tends to infinity:

$$\lim_{n\to\infty} \mathcal{R}(n) = \lim_{n\to\infty} \frac{1}{\sqrt[\gamma]{1/r_0^{\gamma}+n}} \cong n^{-1/\gamma} \tag{14}$$

The parameter γ can be determined experimentally or numerically from plots $\mathcal{R}=f(n)$ on a logarithmic scale by a least squares approximation. The slope of the curve using a logarithmic scale is $-1/\gamma$ (see Figs. 8 and 9).

For the circular contact, the γ obtained numerically by the relation (14), with only two or with fifty passes considered, differs by less than 4%. These results are very close to those obtained by the three point approximation (Table 2) for every oil layer thickness. The difference in the value of γ between the three point approximation and the film decay is 6%. Taking a closer look, the γ profile across the contact width is almost constant.

For the elliptical contact, the γ profile across the contact width shows larger variations. The γ obtained from the three point graph approximation with $r \simeq 1$ is close to the γ obtained by the film decay during the first few passes. The difference is less than 7 percent.

However, the γ value obtained after fifty cycles differs significantly from the one obtained after two cycles and by the 3 point approximation with large amounts of oil. The γ obtained by a film decay analysis with large number of cycles is close to those obtained by the three point approximation with thin oil layers. The difference found between both is less than 20%. Furthermore, these values are closer to the experimental γ which is obtained with a large number of passes ($10 < n < 200$).

5 Experimental Approach

An ultrathin film optical interferometry technique was used to measure the EHD film thickness under starved conditions. Unlike

Table 2 γ **obtained with different models**

	$\kappa=1$ $M=100$ $L=10$	$\kappa=0.27$ $M=50.6$ $L=6.26$
3 point approx. $r \simeq 1$	2.97	5.72
overrollings 2 passes	2.91	6.08
overrollings 50 passes	2.8	4.26
experimental	2.8	3.55

conventional interferometry, which has a lower measurement limit of around 80 nm, the ultrathin film technique can measure films down to a few nm. Details of this technique have been reported elsewhere [19] and only a short description will be given here. The contact is formed between a 19.05 mm diameter steel roller (in the rolling direction) and the flat surface of a glass disc. The contact is loaded through the roller which is mounted on a shaft, supported on bearings and driven via a flexible coupling by an electric motor.

The glass disc is coated on the underside with a chromium semi-reflecting coating, on top of which a ''spacer layer'' of transparent silica is deposited. The film thickness in the contact is measured using an optical interferometry method [19]. Film thickness measurements are normally taken from the center of the contact.

A CCD camera attached to a frame grabber was also mounted on the optical system so that images could be taken from the contact region. Tests were run for a circular (ball on disc) and elliptical (crowned roller on disc) geometry. The same lubricant, a high-viscosity poly-α-olefin was used in all experiments. Table 3 summarizes the conditions for both sets of tests.

6 Experimental Results

Figure 7 shows a moderately starved elliptical contact. The inlet meniscus is seen to the left of the contact. The film decay experiments (Figs. 8 and 9) were repeated for a number of different lubrication conditions. The fact that these are straight lines implies that reflow is negligible as explained by Cann et al. [20]. Figure 10 which shows $\gamma = f(\sqrt{M/L})$ combines all experimental results. As expected from the analytical approach, γ increases with $\sqrt{M/L} \propto 1/\bar{S}$ and with larger ellipticities (smaller κ).

7 Discussion

In Figs. 11 and 12, the filled points show the experimental results whereas the lines and the open symbols show numerical results. The difference between theory and experiments is smaller than 20% for the circular contact. For the elliptical contact, the

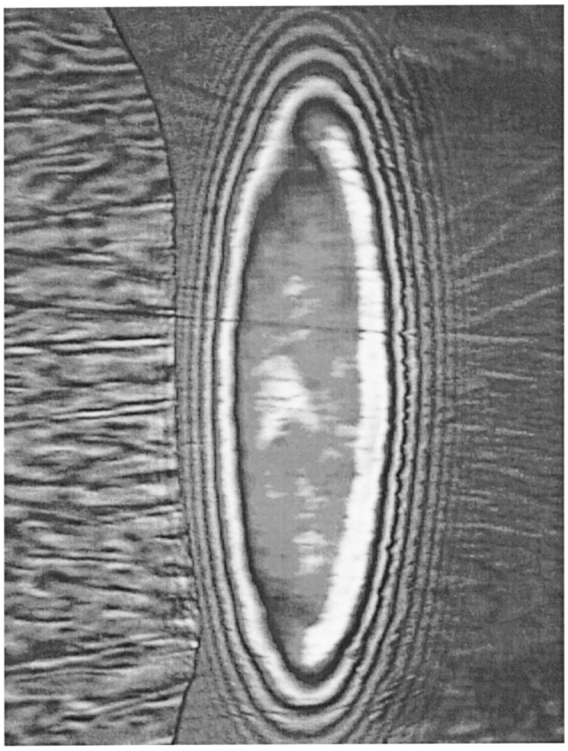

Fig. 7 Starved elliptical contact

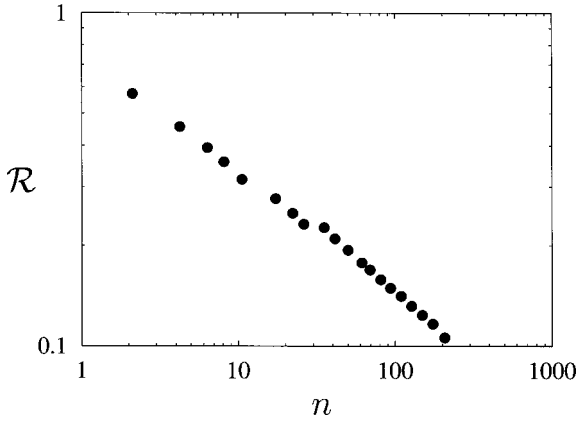

Fig. 8 Experimental film decay for a circular contact $\kappa=1$ ($u_m=96.6$ mms^{-1})

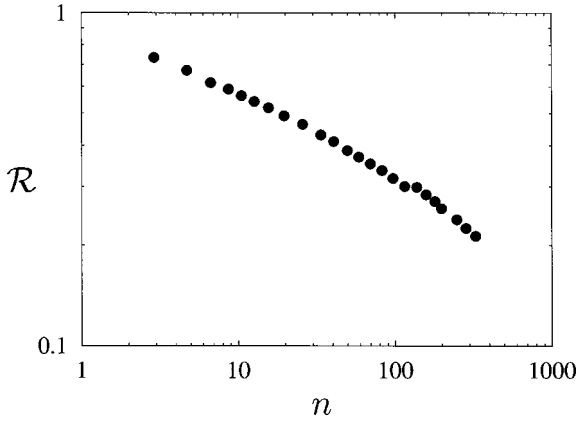

Fig. 9 Experimental film decay for an elliptical contact $\kappa=0.270$ ($u_m=39.8$ mms^{-1})

Table 3 EHL test conditions

Geometry	Circular	Elliptical
test piece	ball $\kappa=1$ $R_x=9.525$ mm $R_y=9.525$ mm	roller $\kappa=0.27$ $R_x=9.525$ mm $R_y=70.0$ mm
p_h	0.51 GPa	0.33 GPa
speed	0.01–1 m/s	0.1–0.32 m/s
T°	25°C	25°C
η_0	0.8 Pa.s	0.8 Pa.s
α	18 GPa^{-1}	18 GPa^{-1}

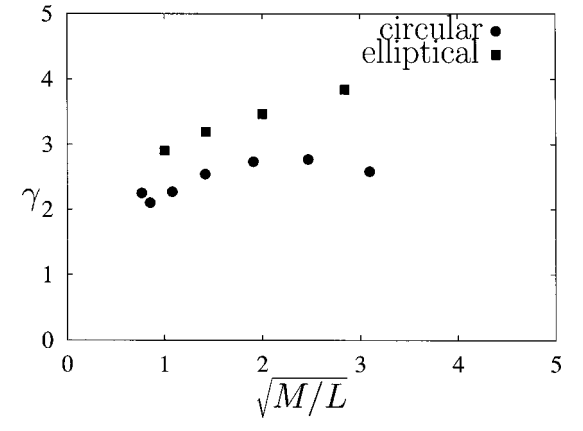

Fig. 10 Experimental γ values as a function of $\sqrt{M/L}$ for a circular ($\kappa=1$) and elliptical ($\kappa=0.27$) contact.

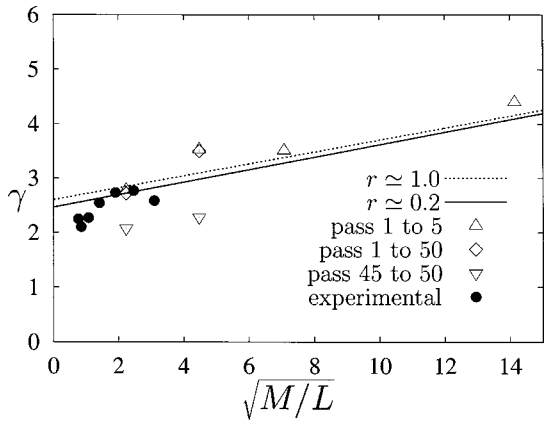

Fig. 11 γ as a function of $\sqrt{M/L}$ for a circular contact $\kappa=1$. Lines and open symbols are numerical predictions.

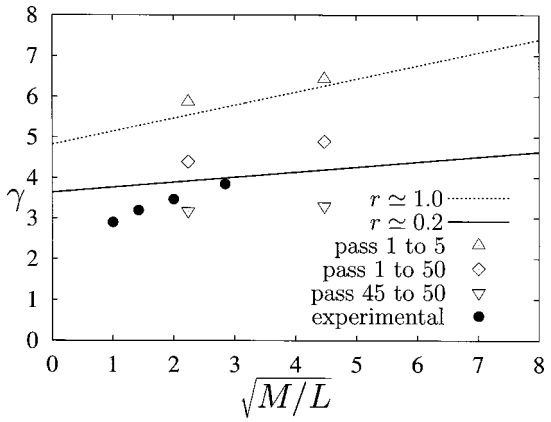

Fig. 12 γ as a function of $\sqrt{M/L}$ for an elliptical contact $\kappa=0.270$. Lines and open symbols are numerical predictions.

difference between experimental and numerical results is less than 25 percent considering that the numerical simulation must be performed with small amounts of oil since the experiments are corresponding large numbers of passes: $10<n<200$.

As expected from the asymptotic behavior (line contact: $\gamma=\infty$), γ increases with increasing ellipticity (κ decreases), (see also Fig. 6). Both the experimental and numerical results show the same trend. The quantitative variations of γ across the contact width depend on the degree of ellipticity. As the configuration becomes more circular the γ variations across the contact decrease. For very large ellipticities on the contrary, each part of the contact is virtually independent of its neighbor.

Figures 11 and 12 show the differences in γ between the different numerical simulations and the experimental results for the circular and the elliptical contact. As expected, the numerical simulations with small amounts of oil are in good agreement with the experimental results: less than 20% difference for the circular contact and less than 25% for the elliptical contact.

8 Conclusion

This paper quantifies starved lubricant film formation as a function of the amount of oil available, the contact conditions and the ellipticity. The ratio M/L proved to be a determinant parameter to predict the side flow. The dimensionless starvation parameter γ derived by Chevalier et al. [1] was used to characterize starvation under different lubrication conditions in the piezoviscous-elastic regime. This starvation parameter γ was linked to the dimensionless inlet length $\overline{S}$. The experimental, analytical, and numerical results, show that the dimensionless parameter γ (side flow resistance) depends on the ratio M/L and is also a function of the oil thickness. A more detailed analysis shows a clear dependence of γ on the amount of oil. As applied by Chevalier in [1] and in Sec. 4.1, the γ behavior in the approximation (13) $\mathcal{R}=f(r)$ is governed by the large amounts of oil ($r\simeq 1$). This value of γ corresponds to the first few cycles. For all operating conditions (M, L, and r) the values of γ can be gathered on one single curve. According to the numerical results and the experimental results for the roller, the curve linking γ to $\sqrt{M/L}$ seems to be a straight line depending on the ellipticity and the amount of lubricant. The maximum difference in γ between experimental and numerical results is about 20 percent for circular and elliptical contact. The value of γ proved to be more dependent on the parameter r for the elliptical contact, and as such Eq. (13) looses some of its appeal for elliptical contacts.

Acknowledgments

The authors would like to thanks PCS Instruments for supplying the optical EHL device and bearing roller test piece.

Nomenclature

a = ellipse axis in rolling direction, $a=(3wR/E')^{1/3}(2\kappa\mathcal{E}/\pi)^{1/3}$
b = ellipse axis perpendicular to rolling direction, $b=a/\kappa=(3wR/E')^{1/3}(2\kappa\mathcal{E}/\pi)^{1/3}/\kappa$
C_{ep} = elastic piezoviscous asymptote coefficient [9], $C_{ep}=2^{17/12}3^{-35/4}\pi^{5/6}\kappa^{-1/12}\lambda^{1/24}(\mathcal{E}/(1+\lambda))^{5/12}$
$\mathcal{D}$ = domain $X_0\leqslant X\leqslant X_e$, $-Y_0\leqslant Y\leqslant Y_0$
E' = reduced modulus of elasticity, $2/E'=(1-\nu_1^2)/E_1+(1-\nu_2^2)/E_2$
G = material parameter, $G=\alpha E'$
h = film thickness
h_c = central film thickness
H = dimensionless film thickness, $H=h(2R\mathcal{E})/(a^2\mathcal{K})$
H_c = dimensionless central film thickness
H_{cff} = dimensionless fully flooded central film thickness
H_0 = dimensionless rigid body displacement
H_{oil} = dimensionless inlet oil film thickness
L = dimensionless material parameter (Moes), $L=G(2U)^{1/4}$
m = parameter of the elliptic integrals $\mathcal{K}$ and $\mathcal{E}$, $m=(1-\kappa^2)^{1/2}$
M = dimensionless load parameter (Moes), $M=W(2U)^{-3/4}$
n = number of disk revolutions (overrollings)
p = pressure
p_h = maximum Hertzian pressure, $p_h=(3w)/(2\pi ab)$
p_0 = constant (Roelands), $p_0=1.96\ 10^8$
P = dimensionless pressure, $P=p/p_h$
R = reduced radius of curvature, $R=(R_x^{-1}+R_y^{-1})^{-1}$
R_x = reduced radius of curvature in x direction, $R_x=(R_{x1}^{-1}+R_{x2}^{-1})^{-1}$
R_y = reduced radius of curvature in y direction, $R_y=(R_{y1}^{-1}+R_{y2}^{-1})^{-1}$, $R_x/R_y=\kappa^2(\mathcal{K}-\mathcal{E})/(\mathcal{E}-\kappa^2\mathcal{K})$
r = relative oil film thickness, $r=H_{\text{oil}}/(\overline{\rho}H_{cff})$
$\mathcal{R}$ = central film thickness reduction, $\mathcal{R}=H_c/H_{cff}$
s = inlet length
s_{ff} = fully flooded inlet length
$\overline{S}$ = dimensionless inlet length $\overline{S}=s_{ff}/a$
u_m = mean velocity in x, $u_m=(u_1+u_2)/2$
U = dimensionless speed parameter, $U=(\eta_0 u_m)/(E'R_x)$
w = external load
W = dimensionless load parameter, $W=w/(E'R_x^2)$
X, Y = dimensionless coordinates, $X=x/a$, $Y=y/b$

X_0, X_e, Y_0 = dimensionless domain boundaries, $X_0 = x_0/a, X_e = x_e/a, Y_0 = y_0/b$
z = pressure viscosity index (Roelands)
α = pressure viscosity coefficient
$\overline{\alpha}$ = dimensionless parameter $\overline{\alpha} = \alpha p_h$, $\overline{\alpha} = L/\pi(3M\pi^2\kappa/2(1+R_x/R_y)^2/16\mathcal{E}^2)^{1/3}$
γ = dimensionless film reduction parameter
λ = dimensionless parameter, $\lambda = \pi(128/3M^4 16\pi\mathcal{E}^5/\kappa^4(1+R_x/R_y)^5\mathcal{K}^6)^{1/3}$
η_0 = viscosity at ambient pressure
$\overline{\eta}$ = dimensionless viscosity, $\overline{\eta} = \eta/\eta_0$
ν_1, ν_2 = poisson ratio of bodies 1 and 2
ρ = density
ρ_0 = density at atmospheric pressure
$\overline{\rho}$ = dimensionless density, $\overline{\rho} = \rho/\rho_0$
θ = filling rate, ratio of oil film thickness and gap height
κ = ellipticity ratio $\kappa = a/b$
$\mathcal{K}(m)$ = $\int_0^{\pi/2} 1\sqrt{1-m^2\sin^2(\psi)}d\psi$
$\mathcal{E}(m)$ = $\int_0^{\pi/2}\sqrt{1-m^2\sin^2(\psi)}d\psi$
$\mathcal{S}$ = $(\mathcal{E}-\kappa^2\mathcal{K})/(\mathcal{K}-\kappa^2\mathcal{K})$

Appendix

A Precision. An error in γ induces an error in the relative film thickness $\mathcal{R}$. Figure 13 shows $\mathcal{R}$ as a function of γ and r. For a given oil layer thickness r and two γ values, the difference in $\mathcal{R}$ can be evaluated. For a given variation in γ, the maximum error in the film thickness $\mathcal{R}$ is obtained for $r=1$. For $2<\gamma<6$, the maximum error in $\mathcal{R}$ is 17 percent.

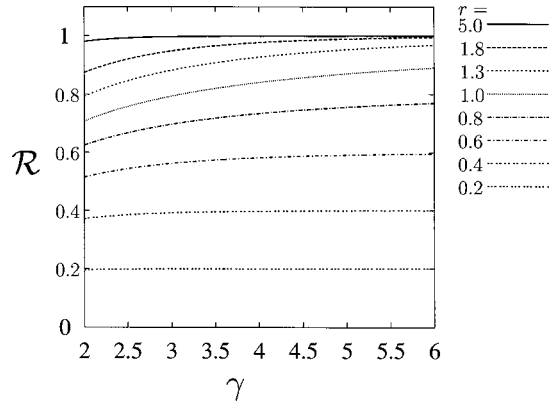

Fig. 13 $\mathcal{R}$ as a function of γ and r

References

[1] Chevalier, F., Lubrecht, A. A., Cann, P. M. E., Colin, F., and Dalmaz, G., 1998, "Film Thickness in Starved EHL Point Contacts," ASME J. Tribol., **120**, pp. 126–133.
[2] Dowson, D., and Higginson, G. R., 1959, "A Numerical Solution to the Elastohydrodynamic Problem," J. Mech. Eng. Sci., **1**, pp. 6–15.
[3] Hamrock, B. J., and Dowson, D., 1976, "Isothermal Elastohydrodynamic Lubrication of Point Contacts, Part I, Theoretical Formulation," ASME J. Lubr. Technol., **98**, pp. 223–229.
[4] Wedeven, L. D., Evans, D., and Cameron, A. C., 1971, "Optical Analysis of Ball Bearing Starvation," ASME J. Lubr. Technol., **93**, pp. 349–363.
[5] Pemberton, J., and Cameron, A. C., 1976, "A Mechanism of Fluid Replenishement in Elastohydrodynamic Contacts," Wear, **37**, pp. 185–190.
[6] Kingsbury, E., 1973, "Cross Flow in a Starved EHD Contact," ASLE Trans., **16**, pp. 276–280.
[7] Chiu, Y. P., 1974, "An Analysis and Prediction of Lubricant Starvation in Following Contact Systems," ASLE Trans., **16**, pp. 276–280.
[8] Guangteng, G., Cann, P. M. E., and Spikes, H. A., 1992, "A Study of Parched Lubrication," Wear, **153**, pp. 91–105.
[9] Moes, H., 2000, "Lubrication and Beyond," technical report, code 115531, University of Twente, Enschede, The Netherlands.
[10] Elrod, H. G., 1981, "A Cavitation Algorithm," ASME J. Lubr. Technol., **103**, pp. 350–354.
[11] Elrod, H. G., and Adams, M. L., 1974, "A Computer Program for Cavitation and Starvation Problems," *Proceedings of the 1st Leeds-Lyon Symposium on Tribology*, pp. 37–41.
[12] Wijnant, Y. H., 1998, "Contact Dynamics in the Field of Elastohydrdynamic Lubrication," Ph.D. thesis, University of Twente, Enschede, the Netherlands, (ISBN:90-36512239).
[13] Ertel, A. M., 1939, "Hydrodynamic Lubrication Based on New Principles," *Akad. Nauk SSSR Prikadnaya Mathematica i Mekhanika*, **3**(2), pp. 41–52.
[14] Grubin, A. N., 1949, *Fundamentals of the Hydrodynamic Theory of Lubrication of Heavily Loaded Cylindrical Surfaces*, Central Scientific Research Institute for Technology and Mechanical Engineering, Book no. 30, Moscow, D.S.I.R. translations.
[15] Wedeven, L. D., 1970, "Optical Measurements in Elastohydrodynamic Rolling-Contact Bearings," Ph.D. thesis, Imperial College, London.
[16] Hooke, C. J., and Venner, C. H., 2000, "Surface Roughness Attenuation in Line and Point Contacts," Proc. Inst. Mech. Eng., **214**, pp. 439–444.
[17] Venner, C. H., and Lubrecht, A. A., 2000, *MultiLevel Methods in Lubrication*, Elsevier (ISBN 0-444-50503-2).
[18] Chevalier, F., 1996, "Modélisation des Conditions d'Alimentation dans les Contacts EHD Ponctuels," Ph.D. thesis, INSA-LYON.
[19] Johnston, G. J., Wayte, R., and Spikes, H. A., 1991, "The Measurement and Study of Very Thin Lubricant Films in Concentrated Contacts," STLE Tribol. Trans., **34**, pp. 187–194.
[20] Cann, P. M. E., and Chevalier, F., and Lubrecht, A. A., 1996, "Track Depletion an Replenishement in a Grease Lubricated Point Contact: A Quantitative Analysis," Leeds-Lyon Symposium on Tribology, pp. 405–414.